Thermal Mechanisms of Millimeter-Wave Stimulation of Excitable Cells

Mikhail G. Shapiro,[†‡§△]* Michael F. Priest,[¶‖△] Peter H. Siegel,[††‡‡] and Francisco Bezanilla[‖]*

[†]Miller Research Institute, [‡]Department of Bioengineering, and [§]Department of Molecular and Cell Biology, University of California, Berkeley, CA; [¶]Committee on Neurobiology and [‖]Department of Biochemistry and Molecular Biology, University of Chicago, Chicago, IL; and [††]Jet Propulsion Laboratory and [‡‡]Department of Biology, California Institute of Technology, Pasadena, CA

Submitted March 21, 2013, and accepted for publication May 07, 2013.

[△]Mikhail G. Shapiro and Michael F. Priest contributed equally to this work.

*Correspondence: mikhail@cheme.caltech.edu or fbezanilla@peds.bsd.uchicago.edu

SUPPORTING MATERIAL

Contents:

Details of the FDTD simulations

Since it was not possible to measure the RF power level and distribution directly (no well-matched biocompatible or immersion probes are available at this wavelength or on a scale compatible with the oocyte dimensions) the actual power density (milliwatts/mm^2) at various positions along the optical path and in the surrounding fluid had to be inferred through electromagnetic simulations of the physical structures composing the RF delivery system, sample chamber, bath fluid and the oocyte itself. A widely utilized numeric Finite Difference Time Domain (FDTD) software (Quickwave, QWED Inc., Warsaw, Poland) was employed for this purpose. The exact physical structure of the test set up, from waveguide port through to the top of the test chamber, including the sample chamber, bath fluid and oocyte itself, was reproduced within the FDTD simulator. Pre-measured values at 60 GHz for the real part of the dielectric constant, ε_r, and conductivity, σ, of the quartz (ε_r=3.8, σ=0), buffer solution (ε_r=12.4, σ=71.3), and oocyte ($\varepsilon_r \approx 12$, $\sigma \approx 60$), were used. The FDTD code was run under several meshing conditions and under a range of frequencies to make sure there were no scale errors or resonances. The power distribution and absolute magnitude of the power density (mW/mm^2) were displayed across the a large area containing the oocyte to see if the distribution was uniform and how much power reached various levels (after reflection and absorption losses) from the bottom to the top of the oocyte. Sample plots from the FDTD simulations are shown in Fig. S2. As can be seen, the power distribution was fairly uniform across the scale of the oocyte and we concluded from the analysis that the power density at the bottom of the oocyte was 2.94X lower than at the waveguide port and that at the top of the oocyte the power density decreased by another 18.3X. For the highest power levels used in our experiments (128mW) these values translate to 17.64 mW/mm^2 at the waveguide output, 6.00 mW/mm^2 at the bottom of the oocyte and 0.33 mW/mm^2 at the top of the oocyte. Power densities for other RF intensities used can be scaled from these.

Supplementary Figures

Figure S1

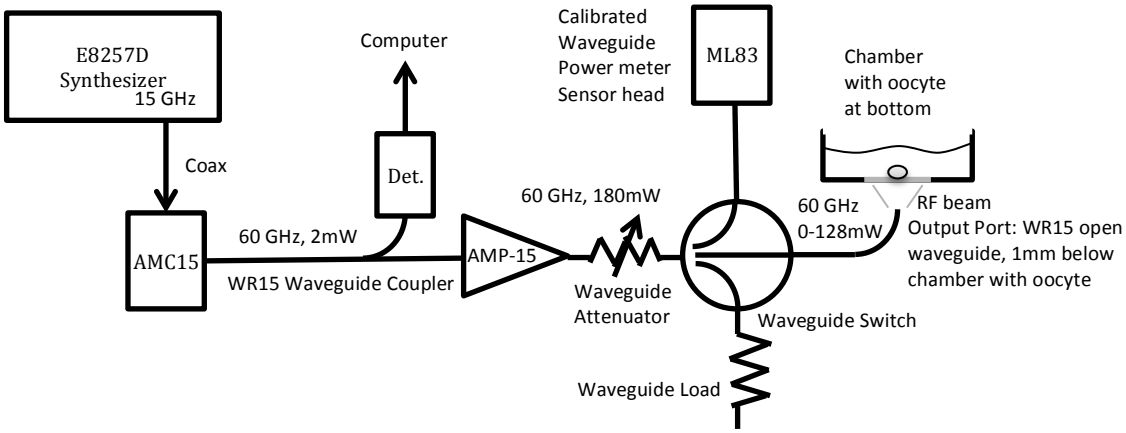

Figure S1. Diagram of the electronic components of the MMW stimulation setup. See Materials and Methods for description.

Figure S2

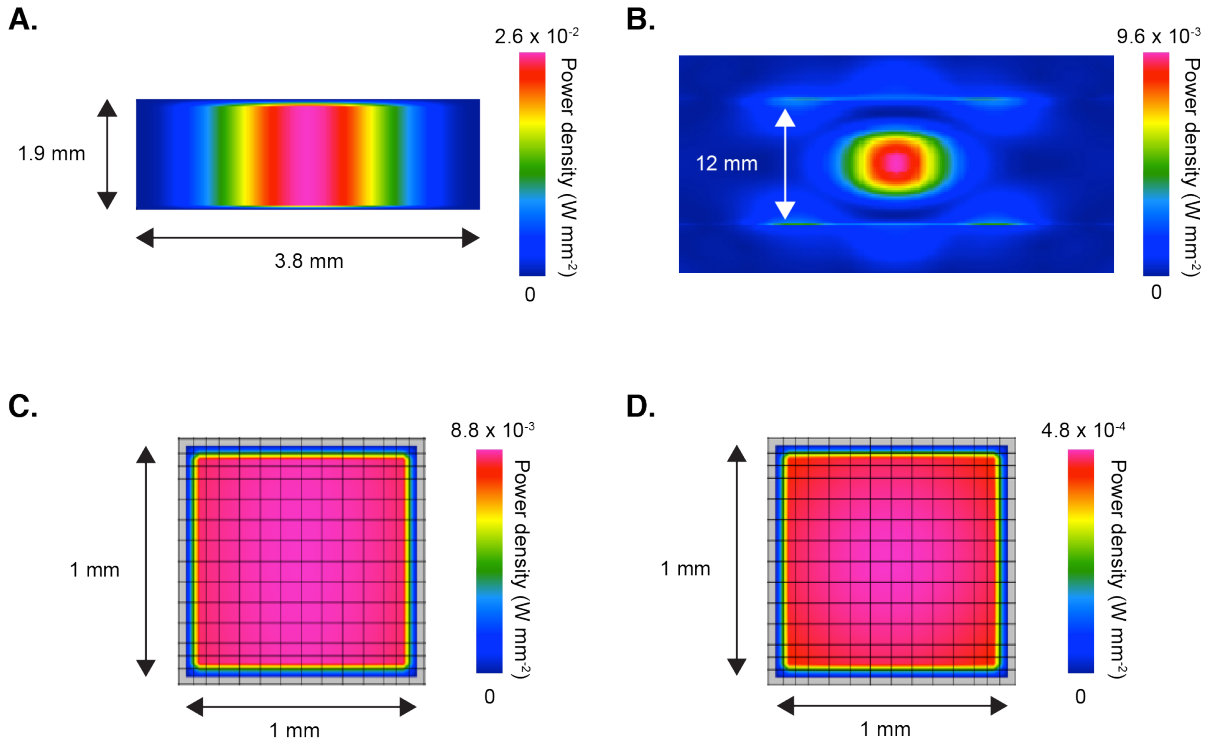

Figure S2. Screen shots of Finite Difference Time Domain (FDTD) simulations of power density distribution at different positions along the RF path. (A) Inside the waveguide, (B) across the middle of the quartz coverslip, (C) at the bottom of the oocyte (1x1mm area) and (D) at the top of the oocyte (1x1mm area). The color maps are linear, with the minimum and maximum as indicated.

Figure S3

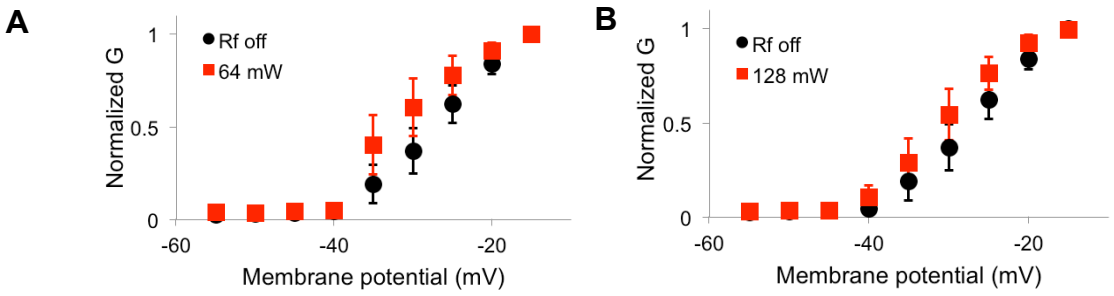

Figure S3. MMW effects on sodium channel conductance. Normalized conductance-voltage response of $Na_v1.4$-injected oocytes with (red) and without (black) MMW stimulation at 64 mW (A) or 128mW (B) N=4. Where error bars (± SEM) are not shown, they are smaller than the symbol.

Figure S4

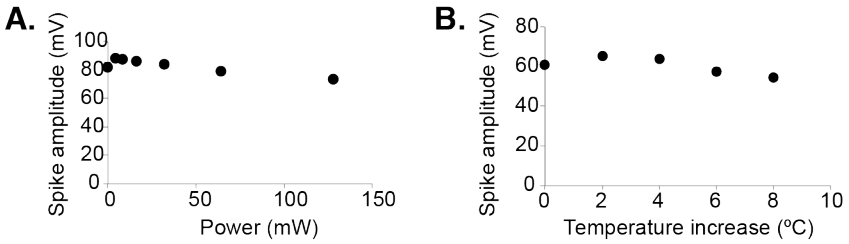

Figure S4. MMW and bath heating alter action potential magnitude. Mean action potential amplitudes recorded in excitocytes exposed to MMW stimulation at the indicated power (A) or to bulk bath heating by the indicated temperature (B). N=4 (A), N=5 (B) and the error bars representing ± SEM are smaller than the symbols in each case.

Figure S5

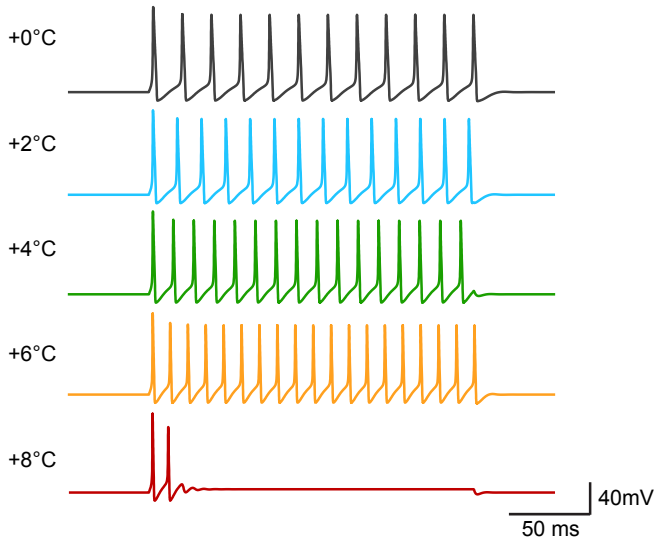

Figure S5. Hodgkin-Huxley model predicts abrogation of action potentials above a certain increase in temperature. Figure identical to Fig. 6, except for the addition of a +8ºC condition. For more information on the kinetic mechanisms underlying this predicted reversible abrogation of action potential firing above a certain temperature, the reader is referred to references 1-2 below.

Supporting References

1 Bezanilla, F., Rojas, E., and R.E. Taylor. (1970). Sodium and potassium conductance changes during a membrane action potential. J. Physiol. 211, 729-751.

2 Rosenthal, J.J. and F. Bezanilla. (2002) A comparison of propagated action potentials from tropical and temperate squid axons: different durations and conduction velocities correlate with ionic conductance levels. J Exp Biol. 205,1819-30.